

## Neural networks for real-time nonlinear control of a variable geometry turbocharged diesel engine

Rabih Omran<sup>1</sup>, Rafic Younes<sup>2,\*</sup>,<sup>†</sup> and Jean-Claude Champoussin<sup>1</sup>

<sup>1</sup>*LMFA, Ecole Centrale de Lyon, Lyon, France*

<sup>2</sup>*Engineering Faculty, Lebanese University, Beirut, Lebanon*

### SUMMARY

New engines are submitted to emission standards that are becoming more and more restrictive. Diesel engines are typically equipped with variable geometry turbo-compressor, exhaust gas recirculation system, high-pressure common rail system and post-treatment devices in order to meet these legislative requirements. Consequently, the control of diesel engines becomes a very difficult task involving five to 10 control variables that interact with each other and that are highly nonlinear. Until the present day, the control schemes integrated in the engine's controller are all based on static maps identified by steady-state engine mapping. Afterward, these schemes are adjusted and calibrated in the vehicle using various control techniques in order to assure a better dynamic response of the engine under dynamic load. In this paper, we are interested in developing a mathematical optimization process that searches for the optimal control scheme under static and dynamic operating conditions. Firstly, we suggest modeling the engine and its emissions using mean value models which require limited experiments and are in good agreement with the experimental data. These models are then used in a dynamic optimization process based on the Broyden–Fletcher–Goldfarb–Shanno algorithm in order to find the optimal control scheme of the engine. The results show a reduction of the engine emissions without deteriorating its performance. Finally, we propose a practical control technique based on neural networks in order to apply these control schemes online to the engine. The results are promising. Copyright © 2007 John Wiley & Sons, Ltd.

Received 19 February 2007; Revised 15 June 2007; Accepted 2 July 2007

KEY WORDS: diesel engines; mean value model; dynamic optimization process; optimal control and neural networks

### 1. INTRODUCTION

Diesel engines are typically equipped with control and post-treatment devices [1–5] that are designed to increase engine power and human comfort while reducing harmful engine emissions.

\*Correspondence to: Rafic Younes, Engineering Faculty, Lebanese University, Campus Universitaire de Rafic Hariri, Hadath, Beirut, Lebanon.

<sup>†</sup>E-mail: ryounes@ul.edu.lb

These devices increase the number of the control variables from the two conventional variables (fuel flow rate and crankshaft angular speed) to five to 10 variables, thus making the search for the optimal control scheme highly complex and time consuming. Until the present day, the control of the engine has been based on two-dimensional static maps with entries of crankshaft angular speed and fuel flow rate. These maps cover the whole functioning area of the engine and are iteratively identified from experiments that are performed by static engine mapping. Every control actuator has its own map that gives the primary value to be applied to the actuator. Afterward, these primary values are adjusted online by corrected maps that take into consideration the changes in the engine environment and the evolution of the engine state variables that are measured in real time. Finally, in order to meet the emission standards and to increase the efficiency of the engine and enhance its response under dynamic load, the corrected values are modified using various control techniques [6–8]. These methods are characterized by control parameters that are tuned experimentally over a dynamic test bench by technical personnel. Therefore, control development of the engine is clearly very difficult and time consuming: it involves too many experiments over static and dynamic test benches and highly depends upon the judgment of the experimental staff where we cannot eliminate the possibility for human errors, especially with the rising number of the control variables. Consequently, the need of a reliable optimization tool becomes a necessity that has occupied the engine's producers for the last two decades. Such a process requires the build up of consistent engine and exhaust gas models to replace the expensive experiments and to predict the engine's response when varying the engine's control parameters.

In this paper, we propose to use a mean value model to describe the engine state variables and its exhaust emissions [9–12]. This model is based on the ideal gas state equation, the mass and energy conservation principles, the fundamental principle of the dynamic and semi-empirical equations that describe the relations between the different state variables of the engine. We adopted this modeling technique because it is precise and simple enough to be used in a mathematical optimization process; also, it needs limited experimental data for identifying the model parameters. This model, then, is used in a dynamic optimization process based on the Broyden–Fletcher–Goldfarb–Shanno (B.F.G.S) algorithm [13]. The idea is to find the optimal control variables of the engine over dynamic trajectories in order to create dynamic maps that can be directly applied to the corresponding actuators. This optimization process cannot be used directly in vehicles by a control processor because of its relatively long computation time. For this reason, we used it off-line to create a large database, and then this database was used to create a controller based on neural networks that can be integrated in the Electronic Control Unit (ECU). The neural network is a powerful tool that can be used to approximate any function by simply learning from examples [14–19]. It is accurate and not limited by the number of inputs, and its response is almost instant, which makes it an excellent controller [19].

## 2. PROPOSED METHODOLOGY

Diesel engines can be modeled by two different approaches: the models of knowledge (quasi-static, draining replenishment, semi-mixed, bond graph) and the models of representation (transfer functions, temporal series, neural networks). In this paper, we choose the quasi-static mean value model which is the simplest analytic model that can be treated in an optimization process. The engine is divided into several blocks (Appendix A) where the gas states, crankshaft and turbocharger

angular speed can be described by their differential equations; these equations are deduced from the physical laws governing their movement and transformations and by expressing their characteristic variables in semi-empirical equations identified from static experimental data. Once the parameters of the model are identified from the experimental data and the model is validated to correctly predict the engine behavior, it can be integrated in a dynamic optimization process that aims at finding the optimal control variables over dynamic trajectories. These trajectories are chosen arbitrarily in order to cover the whole functioning area of the engine. The created database is then used to train a neural network in order to predict the optimal control variables in engine real-time operations. Thus, the memorized maps are replaced by the values of the weights and bias of the neural network controller. Consequently, the proposed methodology can be divided into eight steps:

1. Experimental data acquisition.
2. Engine and exhaust gas modeling.
3. Model validation, in which model simulations are compared with experimental data taken over dynamic trajectories.
4. Dynamic optimization process concept and validation.
5. Creation of a large database of the optimal control variables using the dynamic optimization process.
6. Creation of the neural network.
7. Validation of the neural control.
8. Integration of the neural network controller into the engine model simulations: testing the prediction capacity of the controller in real-time simulations.

### 3. ENGINE AND OPACITY MODELING

The test bench used for data acquisition employs a six-cylinder turbocharged diesel engine (Figure 1), a brake dynamometer, a Bosch smoke detector and various sensors to measure the gas state variables in the different blocks of the engine. The engine characteristics are reported in Table I.

The complete model is characterized by six principal state variables ( $p_a$ ,  $m_a$ ,  $p_e$ ,  $m_e$ ,  $w$  and  $w_{tc}$ ), three inputs ( $\dot{m}_f$ ,  $C_r$  and GV) and the following six differential equations representing the

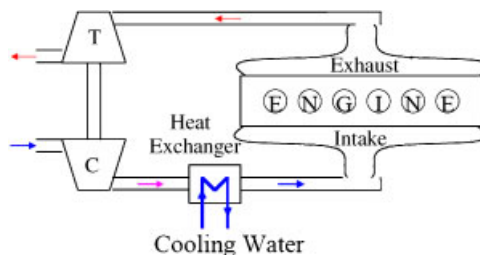


Figure 1. Schematic description of the engine setup.

Table I. Engine characteristics.

Stroke (mm)	145
Displacement [l]	9.84
Volumetric ratio	17/1
Bore (mm)	120
Maximum power (kW) at crankshaft angular speed (rpm)	260
	2400
Maximum torque (N m) at crankshaft angular speed (rpm)	1580
	1200
Relative boost pressure (bar)	2

dynamic processes in the different engine blocks (Appendix A):

$$\begin{aligned}
 p_{a(i+1)} - p_{a(i)} - \frac{\gamma_a \cdot R \cdot h}{V_a} \cdot (\dot{m}_{c(i)} \cdot T_{HE(i)} - \dot{m}_{ai(i)} \cdot T_{a(i)}) &= 0 \\
 m_{a(i+1)} - m_{a(i)} - h \cdot (\dot{m}_{c(i)} - \dot{m}_{ai(i)}) &= 0 \\
 p_{e(i+1)} - p_{e(i)} - \frac{\gamma_e \cdot R \cdot h}{V_e} \cdot (\dot{m}_{t(i)} \cdot T_{e(i)} - \dot{m}_{e0(i)} \cdot T_{x(i)}) &= 0 \\
 m_{e(i+1)} - m_{e(i)} - h \cdot (\dot{m}_{ai(i)} + \dot{m}_{f(i)} - \dot{m}_{t(i)}) & \\
 w_{(i)} \cdot (w_{(i+1)} - w_{(i)}) - \frac{h}{J} \cdot (\eta_{e(i)} \cdot \dot{m}_{f(i)} \cdot H_f - C_{r(i)} \cdot w_{(i)}) &= 0 \\
 w_{tc(i)} \cdot (w_{tc(i+1)} - w_{tc(i)}) - \frac{h}{I_{tc}} \cdot (\eta_m P_{t(i)} - P_{c(i)}) &= 0
 \end{aligned} \tag{1}$$

The pollutants that characterize diesel engines are mainly oxides of nitrogen and the particulate matter. In this paper, we are only interested in presenting the optimization process and its advantages without complicating the models; hence we choose the opacity as a pollution criterion expressed by the following semi-empirical equation:

$$\text{Opacity} = m_1 \cdot w^{m_2} \cdot \dot{m}_{ai}^{m_3 \cdot w + m_4} \cdot \dot{m}_f^{m_5 \cdot w + m_6} \tag{2}$$

$m_i$  are constants identified from the experimental data.

The results of the model simulations are compared with the experimental data measured on the test bench while simultaneously changing in the three inputs, the fuel flow rate, the position of the variable geometry turbo-compressor and the friction torque. Figure 2 illustrates a comparison between the complete model simulation results and the experimental data of the engine under dynamic load; they are in excellent agreement.

## 4. DYNAMIC OPTIMIZATION PROCESS

### 4.1. Problem statement

When conceiving and producing a new engine, developers and mechanical engineers have always to confront and properly solve the contradictory problem of producing maximum power (or minimum

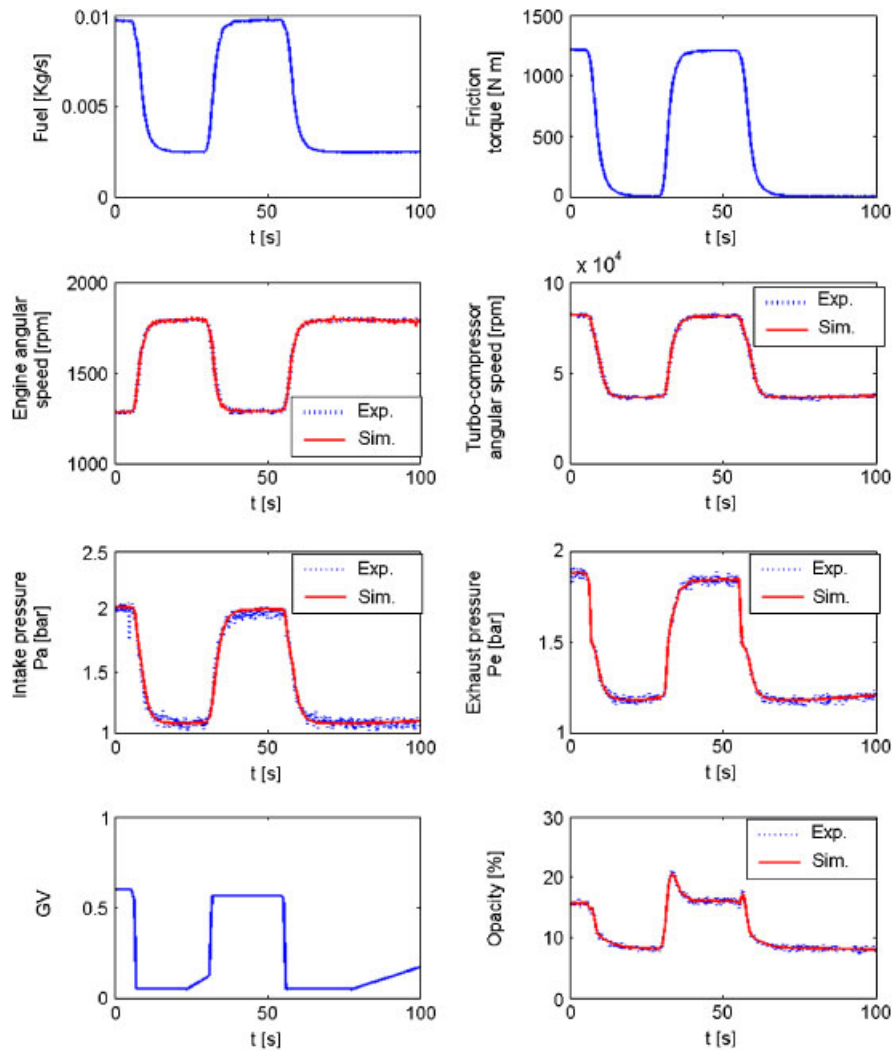


Figure 2. Comparison between the simulations and the experimental data.

fuel consumption) while meeting emission regulations. In vehicles, emission control classically takes two forms:

1. Engine output control, by regulating fuel and exhaust gas recirculation, for example.
2. After treatment control, by catalysis such as selective catalytic reduction and devices such as particulate traps, for example.

In this paper, we are only interested in resolving the pollution problem at the engine level, by searching for the optimal control variables that minimize a desired function. Consequently, the

problem can now be defined; it consists of the following multi-criteria function:

$$\begin{aligned} &\text{Maximize 'Power'} \\ &\text{Minimize 'Pollutants'} \end{aligned} \tag{3}$$

Considering that passenger car engines usually run under dynamic load, an optimization process that searches for the optimal control variables of the engine under steady state would be inefficient. Consequently, we propose a dynamic optimization process that searches for these variables over a dynamic course where the engine inputs are allowed to change. The proposed optimization process can also be used to search for the engine optimal control scheme under static load by simply choosing steady courses. The multi-criteria objective function described in (3) can now be expressed by a single nondimensional mathematical equation defined over a time interval  $[0, t]$ :

$$f = -\int \frac{P}{P_{\max}} dt + \sum_i \left\{ \int \frac{\text{Poll}_i}{\text{Poll}_{i,\max}} dt \right\} \tag{4}$$

where  $P$  is the engine effective power,  $\text{Poll}_i$  is a type of pollutant, and the indication max is the maximum value that a variable can reach. In order to solve the contradictory task of maximizing the effective power and minimizing the pollution at the same time we used a minus sign before the power term in the objective function. The effective power is a positive number. Therefore, maximizing its value is equivalent to minimizing the same term preceded by a negative sign. The integral represents the accumulated pollutants and power over the dynamic trajectory. In this paper, we will only use the opacity as an indication of the pollution in order to simplify the model and demonstrate the method, but we should note that the optimization process is universal and it can involve as many pollution criteria as we need

$$(4) \rightarrow f = -\int \frac{P}{P_{\max}} dt + \int \frac{\text{Op}}{\text{Op}_{\max}} dt \tag{5}$$

#### 4.2. Problem formulation

Every optimization problem is defined by specifying the inputs, the optimization variables to be identified, the objective function to be minimized, the equality constraints describing the relationship between the different optimization variables and inputs, and the inequality constraints representing the lower and upper limits of each variable. In our case, the inputs are the fuel flow rate  $\dot{m}_f(t)$  and the friction torque  $C_r(t)$ , the optimization variables are:  $p_a(t)$ ,  $m_a(t)$ ,  $p_e(t)$ ,  $m_e(t)$ ,  $w(t)$ ,  $w_{tc}(t)$  and  $\text{GV}(t)$ . The objective function is computed using (2) and using (A16) and (A17) in Appendix A:

$$f = \left\{ \begin{aligned} &-\frac{H_f}{P_{\max}} \cdot \int \eta_e \cdot \dot{m}_f dt \\ &+\frac{m_1}{\text{Op}_{\max}} \cdot \int w^{m_2} \cdot \dot{m}_{ai}^{m_3 \cdot w + m_4} \cdot \dot{m}_f^{m_5 \cdot w + m_6} dt \end{aligned} \right\} \tag{6}$$

The equality constraints are differential equations (1) representing the dynamic behavior of the engine. The inequality constraints represent the physical and mechanical limits that the air to fuel ratio, the intake pressure, the exhaust pressure, the engine angular speed and the turbocompressor

angular speed must respect:

$$\begin{aligned}
 15 &\leq \lambda \leq 80 \\
 9.5 \cdot 10^4 &\leq p_a \leq 30 \cdot 10^4 \quad [\text{Pa}] \\
 9.5 \cdot 10^4 &\leq p_e \leq 30 \cdot 10^4 \quad [\text{Pa}] \\
 83 &\leq \omega \leq 230 \quad [\text{rd/s}] \\
 2 \cdot 10^3 &\leq \omega_{tc} \leq 13 \cdot 10^3 \quad [\text{rd/s}]
 \end{aligned} \tag{7}$$

#### 4.3. Problem discretization

The problem previously described is highly nonlinear; the analytic solution is clearly unrealistic. Therefore, it is necessary to reformulate the problem in its discretized form. The time interval is discretized to  $N$  points  $t_i$  using a time step  $h$ . The integrals in (6) become simple sums of the integrated functions at different instants  $t_i$ :

$$f = \left\{ \begin{array}{l} -\frac{H_f}{P_{\max}} \cdot \sum_{i=1}^N (\eta_e \cdot \dot{m}_f)_{(i)} \\ +\frac{m_1}{Op_{\max}} \cdot \sum_{i=1}^N (w^{m_2} \cdot \dot{m}_{ai}^{m_3 \cdot w + m_4} \cdot \dot{m}_f^{m_5 \cdot w + m_6})_{(i)} \end{array} \right\} \tag{8}$$

The equality constraints described in (1) are computed using the Taylor series truncated at first differential order:

$$\left. \begin{array}{l} p_{a(i+1)} - p_{a(i)} - \frac{\gamma_a \cdot R \cdot h}{V_a} \cdot (\dot{m}_{c(i)} \cdot T_{HE(i)} - \dot{m}_{ai(i)} \cdot T_{a(i)}) = 0 \\ m_{a(i+1)} - m_{a(i)} - h \cdot (\dot{m}_{c(i)} - \dot{m}_{ai(i)}) = 0 \\ p_{e(i+1)} - p_{e(i)} - \frac{\gamma_e \cdot R \cdot h}{V_e} \cdot (\dot{m}_{t(i)} \cdot T_{e(i)} - \dot{m}_{e0(i)} \cdot T_{x(i)}) = 0 \\ m_{e(i+1)} - m_{e(i)} - h \cdot (\dot{m}_{ai(i)} + \dot{m}_{f(i)} - \dot{m}_{t(i)}) = 0 \\ w_{(i)} \cdot (w_{(i+1)} - w_{(i)}) - \frac{h}{J} \cdot (\eta_{e(i)} \cdot \dot{m}_{f(i)} \cdot H_f - C_{r(i)} \cdot w_{(i)}) = 0 \\ w_{tc(i)} \cdot (w_{tc(i+1)} - w_{tc(i)}) - \frac{h}{I_{tc}} \cdot (\eta_m P_{t(i)} - P_{c(i)}) = 0 \end{array} \right\} \tag{9}$$

The inequality constraints described in (7) are also expressed by their discretized form:

$$\begin{aligned}
 15 &\leq \lambda_{(i)} \leq 80 \quad [ ] \\
 9.5 \cdot 10^4 &\leq p_{a(i)} \leq 30 \cdot 10^4 \quad [\text{Pa}] \\
 9.5 \cdot 10^4 &\leq p_{e(i)} \leq 30 \cdot 10^4 \quad [\text{Pa}] \\
 83 &\leq \omega_{(i)} \leq 230 \quad [\text{rd/s}] \\
 2 \cdot 10^3 &\leq \omega_{tc(i)} \leq 13 \cdot 10^3 \quad [\text{rd/s}]
 \end{aligned} \tag{10}$$

#### 4.4. Optimization algorithm

An optimization problem is usually defined using the following mathematical form:

$$\begin{aligned}
 & \text{Min}\{f(X)\} \\
 & X = (x_1, x_2, \dots, x_n) \\
 & \text{Under Constraints} \\
 & h_i(X) = 0, \quad i = 1, \dots, m \\
 & g_i(X) \leq 0, \quad i = 1, \dots, p
 \end{aligned} \tag{11}$$

where  $f(X)$  is the objective function,  $h(X)$  the equality constraints and  $g(X)$  the inequality constraints. The first step in resolving this problem is to reduce it to a problem without constraints by creating a global objective function  $\Phi(X, r)$  which regroups the original objective function and the equality and inequality constraints multiplied by a penalty number  $r$

$$\phi(X, r) = f(X) + r \cdot \sum_{i=1}^m [h_i(X)]^2 + r \cdot \sum_{i=1}^p [G_i(X)]^2 \tag{12}$$

$$G_i(X) = \begin{cases} g_i(X) & \text{if } g_i(X) > 0 \\ 0 & \text{if } g_i(X) \leq 0 \end{cases} \tag{13}$$

$$r = r_0^k \tag{14}$$

$k$  is the number of iterations that tends toward infinity, and  $r_0 = 3$  is the initial penalty number. The optimization algorithm adopted in this paper is B.F.G.S. algorithm that sums up as follows (Figure 3):

- (a) Start by an initial solution  $X_i^{(k)}$ ,  $i = 0$  and  $k = 1$ .
- (b) Compute  $X_{i+1}^{(k)}$  using the following equation:

$$X_{i+1}^{(k)} = yX_i^{(k)} - \alpha_i^{(k)} \cdot D_i^{(k)} \cdot \nabla \phi_i^{(k)} \tag{15}$$

$\nabla \phi$  is the gradient computed by differentiating (12) with respect to  $X$ ,  $D$  is an approximation of the inverse of the Hessian matrix calculated using the Armijo–Goldstein approximation:

$$D_{i+1}^{(k)} = \begin{bmatrix} D_i^{(k)} + \frac{(\nabla \phi_{i+1}^{(k)} - \nabla \phi_i^{(k)}) \cdot (\nabla \phi_{i+1}^{(k)} - \nabla \phi_i^{(k)})^T}{(\nabla \phi_{i+1}^{(k)} - \nabla \phi_i^{(k)})^T \cdot (X_{i+1}^{(k)} - X_i^{(k)})} \\ - \frac{D_i^{(k)} \cdot (X_{i+1}^{(k)} - X_i^{(k)}) \cdot (X_{i+1}^{(k)} - X_i^{(k)})^T \cdot D_i^{(k)}}{(X_{i+1}^{(k)} - X_i^{(k)})^T \cdot D_i^{(k)} \cdot (X_{i+1}^{(k)} - X_i^{(k)})} \end{bmatrix} \tag{16}$$

$$D_0^{(k)} = I$$

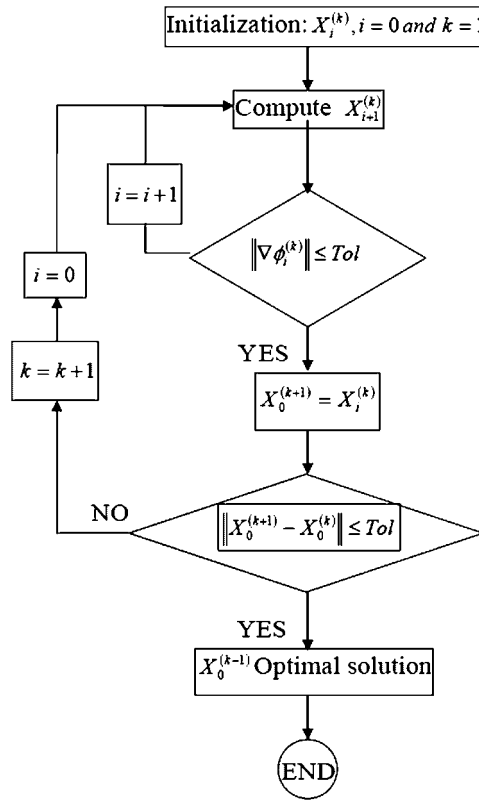


Figure 3. Optimization algorithm.

$\alpha_i^{(k)}$  is the relaxation factor that must respect the Armijo–Goldstein condition:

$$\begin{aligned}
 \phi_i(X_i^{(k)} - \alpha_i^{(k)} \cdot D_i^{(k)} \cdot \nabla\phi_i^{(k)}, r_0^k) &\leq S_i^{(k)} \\
 S_i^{(k)} &= \phi_i^{(k)} - \beta \cdot \alpha_i^{(k)} \cdot [\nabla\phi_i^{(k)}]^T \cdot D_i^{(k)} \cdot \nabla\phi_i^{(k)} \\
 \beta &\in ]0, 1]
 \end{aligned}
 \tag{17}$$

(c) If  $\|\nabla\phi_i^{(k)}\| > \text{Tolerance}$  then :  $i = i + 1$  and goto (b)

(d) If  $\|\nabla\phi_i^{(k)}\| \leq \text{Tolerance}$  then :  $X_0^{(k+1)} = X_i^{(k)}$

If  $\|X_0^{(k+1)} - X_0^{(k)}\| > \text{Tolerance}$  then :  $\left\{ \begin{array}{l} k = k + 1, i = 0 \\ \text{and goto (b)} \end{array} \right\}$

Else: End of search and  $X_0^{(k+1)}$  is the optimal solution

#### 4.5. Results

In this subsection, we present the application of the optimization algorithm explained in the previous section to two different profiles of input variables (fuel mass flow rate and friction torque). The step of discretization  $h$  is equal to 0.01 s and the time interval is equal to 3 s, each problem has 1500 unknown variables with 1196 equality constraints and 3000 inequality constraints. Figures 4 and 5 show a comparison between the results of the optimization process and the simulation's results of the engine's complete model (Appendix A) for fixed geometry turbocharger ( $GV = 0$ ). In Figure 4, the cumulated effective efficiency is increased by 5% and the cumulated opacity is reduced by 68%. In Figure 5, the cumulated effective efficiency is increased by 1% and the cumulated opacity is reduced by 42%.

### 5. OPTIMAL CONTROL DATABASE

The dynamic optimization process explained in Section 6 cannot be integrated 'online' in the Engine Control Unit (ECU) and applied directly to real engine applications because of its long

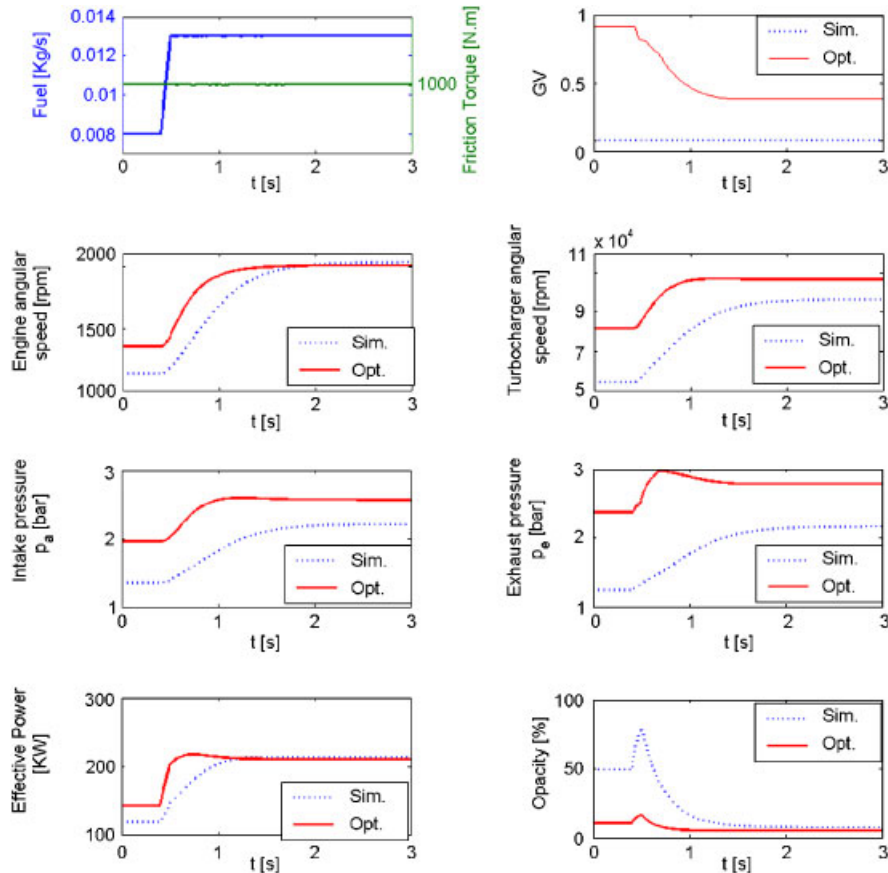


Figure 4. Example 1. Comparison between the optimization results and the complete engine simulations.

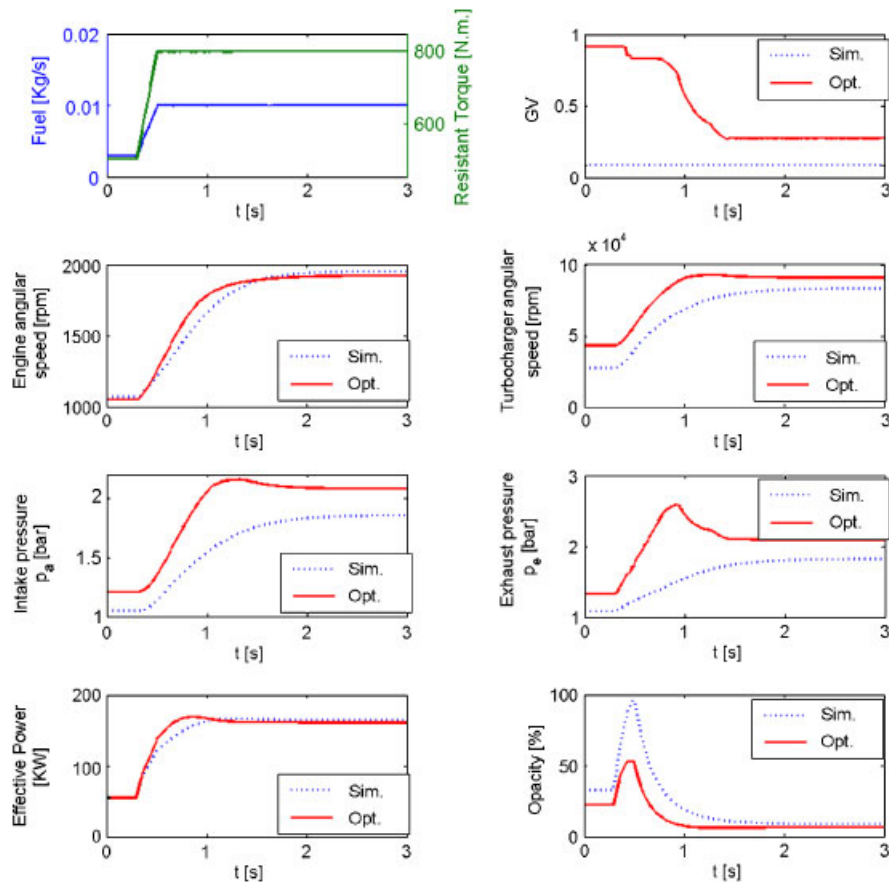


Figure 5. Example 2. Comparison between the optimization results and the complete engine simulations.

computation time. It can be used to construct dynamic maps that cover the whole engine functioning area. Then, these maps can be integrated into the ECU in order to replace the conventional static maps and control schemes as described in the Introduction, but the huge memory size involved makes it unusable in passenger car applications.

Therefore, another approach should be considered. We propose to use neural networks as a control tool to predict online the optimal control variables to be applied to the engine. Neural networks are a powerful tool that can be used for approximating any multiple input–multiple output function; it has the capacity to identify the nonlinear relations between the different inputs and to predict the correct output variables with a desired precision by simply learning from examples. In order to build a network with good prediction accuracy, the database used in the training process must be large enough and must cover the whole functional area of the engine. The trajectories  $\{\dot{m}_f(t), C_r(t)\}$  used to create the database are chosen randomly in a way to respect the inequality constraints as described in (10).

## 6. NEURAL CONTROL

The neural network adopted in this paper is a three-layer perceptron with an input layer, one hidden layer with 50 neurons and an output layer. This type of neural network is commonly used in function approximating problems. The transfer functions at the hidden and the output layer are sigmoid. We also selected the back-propagation algorithm to train the network using the optimal control database; this algorithm uses a sequential method based on the gradient, such as the quasi-Newton algorithm, to adjust the weights and bias of the neurons in a way to minimize a performance function selected as a criterion to reflect the capacity of the model to predict the true outputs. Given its attractive generalization property and its capacity to obtain a stable model, the performance function chosen as a criterion to train our network has the following form:

$$f = \frac{\gamma}{M} \cdot \sum_{i=1}^N e_i^2 + \frac{1-\gamma}{M} \cdot \sum_{i=1}^N w_i^2 \quad (18)$$

where  $e$  is the error between the outputs of the network and the training data,  $w$  is the weights and bias of the neurons,  $M$  is the number of couples (input–output) used in the training data and  $\gamma$  is a real number between zero and one that must be properly chosen to obtain the desired precision. The value of  $\gamma$  equal to one leads to a minimal error between the network outputs and the training data, but the model will not be robust. We continue to decrease this factor until obtaining a model that is sensitive to the variations of the various inputs and that is capable of predicting, with a desired precision, the outputs when it is faced with new inputs that are not used in the training phase.

The inputs of the optimization problem are  $\{\dot{m}_f, C_r\}$  and the exit variables are  $\{p_a, m_a, p_e, m_e, w, w_{tc}, GV\}$ . The entries of the neural network are the engine variables that can be measured online by sensors installed on the engine, the output of the network is the control variable which, are in our case, is the position of the variable geometry turbine GV. The model should also take into account the dynamic behavior of the engine and its influence over the value of GV. Consequently, the neural model (Figure 6) becomes a recurrent model with inputs:

$$\left\{ \begin{array}{l} \dot{m}_f(t_i), w(t_i), p_a(t_i), p_e(t_i), w_{tc}(t_i) \\ \dot{m}_f(t_{i-1}), w(t_{i-1}), p_a(t_{i-1}), p_e(t_{i-1}), w_{tc}(t_{i-1}), GV(t_{i-1}) \\ \dot{m}_f(t_{i-2}), w(t_{i-2}), p_a(t_{i-2}), p_e(t_{i-2}), w_{tc}(t_{i-2}), GV(t_{i-2}) \\ \dot{m}_f(t_{i-3}), w(t_{i-3}), p_a(t_{i-3}), p_e(t_{i-3}), w_{tc}(t_{i-3}), GV(t_{i-3}) \end{array} \right\} \quad (19)$$

The output is  $\{GV(t_i)\}$ . We chose a time step suitable for real-time engine applications and sensors response:

$$t_i - t_{i-1} = 10 \cdot h = 0.1s \quad (20)$$

## 7. NEURAL CONTROL VALIDATION

Figures 7 and 8 show a comparison between the neural network outputs and two examples chosen from the optimal control database: the first one is included in the training data and the second one

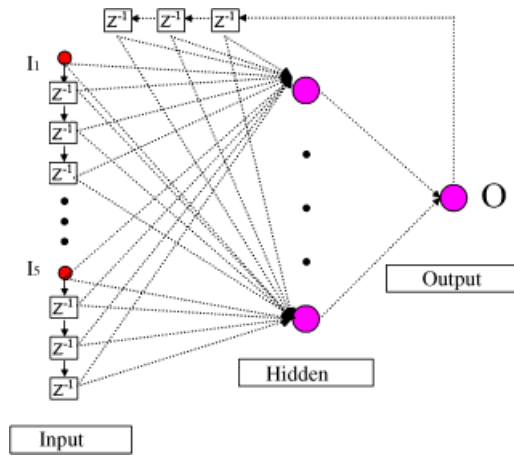


Figure 6. Neural network architecture.

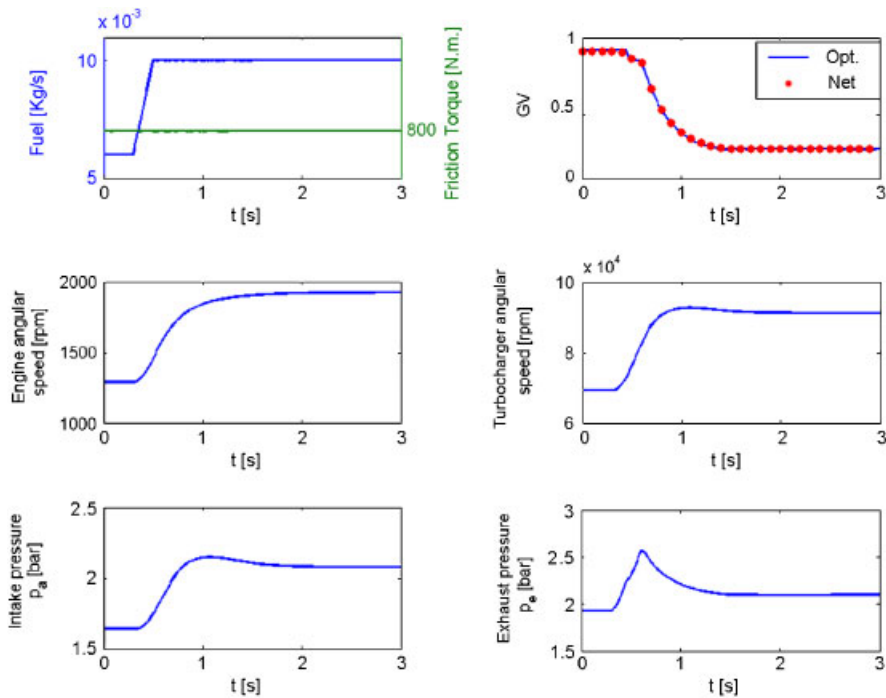


Figure 7. Neural network results. Example used in the training database.

is not, in order to show the capacity of the neural network to predict the optimal control variables when it is faced with new inputs. The results are in excellent agreement with the optimal position of the variable geometry turbine calculated using the optimization process.

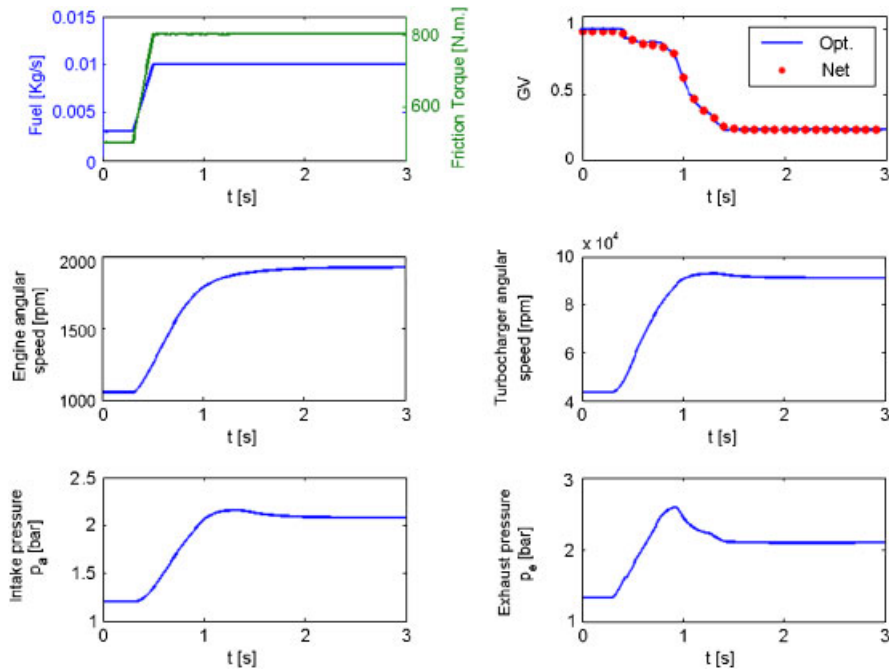


Figure 8. Neural network results. Example not used in the training database.

## 8. INTEGRATION OF THE NEURAL CONTROLLER IN REAL-TIME SIMULATIONS

Figure 9 shows a comparison between an example chosen from the optimal control database and the engine complete model simulation results computed using the outputs of the neural controller that predicts and applies online the optimal opening positions of the turbine variable geometry into the simulations. The neural controller outputs are in good agreement with the optimal opening position found using the dynamic optimization process.

## 9. DISCUSSION

We successfully modeled a variable geometry turbocharged diesel engine and its opacity using the mean value model. The simulation results are in good agreement with the experimental data. The model can be expanded to cover other pollutants, such as carbon monoxide and dioxide, nitrogen oxide and hydrocarbons, using the same approach. This will be the objective of a future paper.

We proposed a mathematical optimization process capable of identifying the optimal control variables over dynamic trajectories. Therefore, expensive experiments are no longer needed, the human error factor is eliminated and the control schemes based on static maps and dynamic correctors are replaced by more efficient dynamic maps that can be applied directly to the control actuators.

Finally, we suggested a neural control that is capable of predicting the optimal control variables to be applied to the engine's actuators and that can be easily integrated in the engine control unit

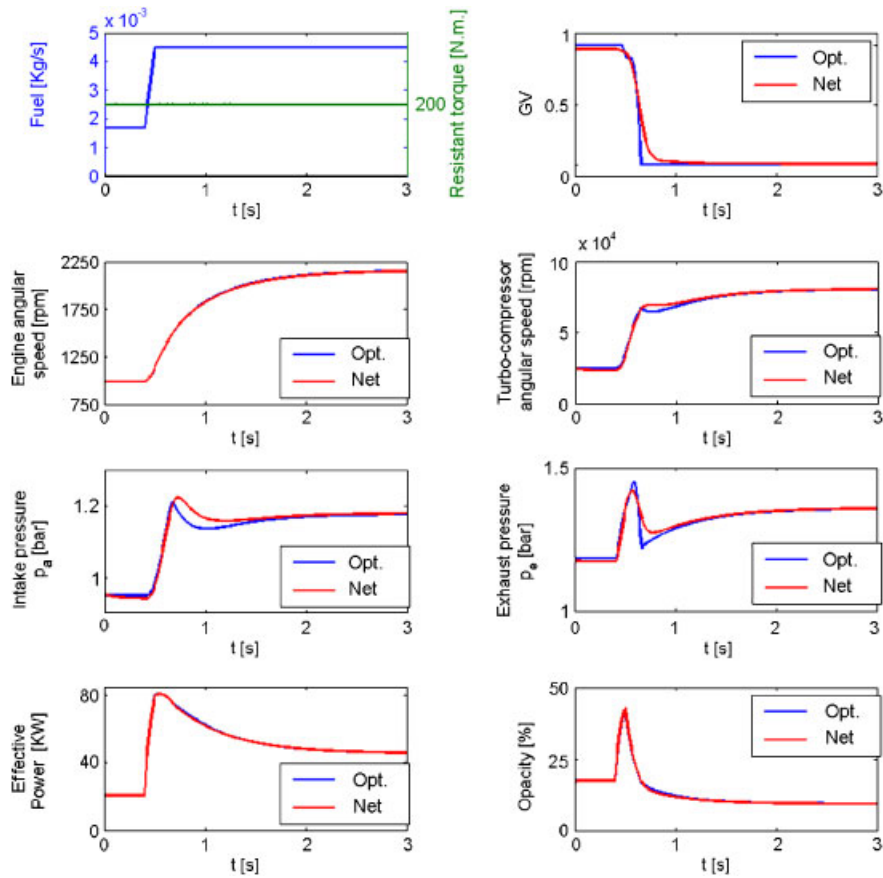


Figure 9. Comparison between the engine complete model simulation results computed using the optimal GV given by the optimization process and the ones computed using the online neural controller.

for real-time applications; the stored maps are then replaced by the weights and bias of the neural control. Also, the proposed architecture of the neural network is indifferent to the number of inputs and outputs involved which makes it a powerful control tool in modern and future diesel engines which may be equipped with variable geometry turbo-compressor, electric compressor, common rail injection system, exhaust gas recirculation system, continuously variable transmission or other devices.

## APPENDIX A

The engine (Figure 1) is divided into four blocks (the intake manifold, the exhaust manifold, the engine and the variable geometry turbo-compressor), each one described by the differential equation governing the dynamic or the gas state changes in the block.

### A.1. Intake manifold

Neglecting the heat losses through the manifold walls and considering the air as an ideal gas with constant specific heats, the differential equation of the intake pressure is computed using the principle of the energy conservation and the ideal gas state equation:

$$\dot{p}_a = \frac{\gamma_a \cdot R}{V_a} \cdot (\dot{m}_c \cdot T_{HE} - \dot{m}_{ai} \cdot T_a) \quad (A1)$$

$\dot{m}_{ai}$  is the air mass flow rate entering the engine and  $T_{HE}$  is the temperature of the air exiting the cooling water heat exchanger.

$$\dot{m}_{ai} \text{ is given by : } \dot{m}_{ai} = \eta_v \cdot \dot{m}_{ai,th} \quad (A2)$$

$\dot{m}_{a0,th}$  is the theoretical air mass flow rate capable of filling the cylinders volume at the pressure and temperature conditions of the intake manifold:

$$\dot{m}_{ai,th} = \frac{N_{cyl} \cdot V_{cyl} \cdot \omega \cdot p_a}{4\pi R T_a} \quad (A3)$$

$\eta_v$  is the inlet air filling efficiency expressed by the semi-empirical equation:

$$\eta_v = \alpha_0 + \alpha_1 \omega + \alpha_2 \omega^2 \quad (A4)$$

where  $\alpha_i$  are constants identified from experimental data. The hot air exiting the compressor is cooled by a water cooled heat exchanger before entering the intake manifold, the temperature  $T_{HE}$  is computed using the following equation:

$$T_{HE} = (1 - \eta_{ech}) \cdot T_c + \eta_{ech} \cdot T_{water} \quad (A5)$$

$T_c$  is the temperature of the air at the compressor's exit,  $T_{water}$  and  $\eta_{ech}$  are, respectively, the temperature of the cooling water and the efficiency of the heat exchanger which are assumed to be constant. The temperature  $T_c$  is deduced from the isentropic efficiency of the compressor:

$$T_c = T_0 \left( 1 + \left( \left( \frac{p_a}{p_0} \right)^{\gamma_a - 1 / \gamma_a} - 1 \right) \frac{1}{\eta_c} \right) \quad (A6)$$

$p_0$  and  $T_0$  are respectively the atmospheric pressure and temperature and  $\eta_c$  is the isentropic efficiency of the compressor. The air mass change in the intake manifold is computed using the mass conservation principle:

$$\dot{m}_a = \dot{m}_c - \dot{m}_{ai} \quad (A7)$$

The temperature of the air in the intake manifold is deduced from the ideal gas state equation:

$$T_a = \frac{p_a \cdot V_a}{m_a \cdot R} \quad (A8)$$

### A.2. Exhaust manifold

Neglecting the heat losses through the manifold walls and considering the exhaust gas as an ideal gas with constant specific heats, the differential equation of the exhaust pressure is computed using the principle of energy conservation and the ideal gas state equation:

$$\dot{p}_e = \frac{\gamma_e \cdot R}{V_e} \cdot (\dot{m}_t \cdot T_e - \dot{m}_{e0} \cdot T_x) \quad (\text{A9})$$

$\dot{m}_t$  is the turbine mass flow rate,  $\dot{m}_{e0}$  is the gas mass flow rate exiting the engine exhaust valves and  $T_x$  is the temperature of the gas exiting the engine.  $\dot{m}_{e0}$  is computed using the following equation:

$$\dot{m}_{e0} = \dot{m}_f + \dot{m}_{ai} \quad (\text{A10})$$

$T_x$  is expressed by the following semi-empirical equation:

$$T_x = T_a + \frac{b_1 + b_2 \cdot \lambda + b_3 \cdot \lambda^2}{1.2 + \frac{\lambda}{15}} + \frac{b_4}{w} + b_5 \quad (\text{A11})$$

$\dot{m}_f$  is the fuel mass flow rate,  $b_i$  are constants identified from experimental data and  $\lambda$  is the air to fuel ratio computed using (A2)–(A4):

$$\lambda = \frac{\dot{m}_{ai}}{\dot{m}_f} = \frac{(\alpha_0 + \alpha_1 \omega + \alpha_2 \omega^2) \cdot N_{\text{cyl}} \cdot V_{\text{cyl}} \cdot \omega \cdot p_a}{4 \cdot \pi \cdot \dot{m}_f} \quad (\text{A12})$$

The gas mass change in the exhaust manifold is computed using the mass conservation principle:

$$\dot{m}_e = \dot{m}_{ai} + \dot{m}_f - \dot{m}_t \quad (\text{A13})$$

The temperature of the gas in the exhaust manifold is deduced from the ideal gas state equation:

$$T_e = \frac{p_e \cdot V_e}{m_e \cdot R} \quad (\text{A14})$$

### A.3. Engine

Applying the principle of the conservation of energy to the crankshaft gives

$$\frac{d}{dt} \left( \frac{1}{2} \cdot J(\theta) \cdot \omega^2 \right) = P_e - P_r \quad (\text{A15})$$

$J(\theta)$  is the moment of inertia of the motor. It is a periodic function of the crankshaft angle due to the repeated motion of its pistons and connecting rods but, for simplicity in this paper, the inertia is considered as a constant.  $P_e$  is the effective power produced by the combustion process:

$$P_e = \eta_e \cdot \dot{m}_f \cdot H_f \quad (\text{A16})$$

$H_f$  is the lower heating value of fuel and  $\eta_e$  is the effective efficiency of the engine expressed by the semi-empirical equation:

$$\eta_e = \lambda \cdot (c_1 + c_2 \cdot \lambda + c_3 \cdot \lambda^2 + c_4 \cdot \lambda \cdot w + c_5 \cdot \lambda^2 \cdot w + c_6 \cdot \lambda \cdot w^2 + c_7 \cdot \lambda^2 \cdot w^2) \quad (\text{A17})$$

where  $c_i$  are constants identified from experimental data.

$P_f$  is the friction power:

$$P_f = C_r \omega \quad (\text{A18})$$

$C_r$  is the friction torque controlled by the dynamometer.

#### A.4. Variable geometry turbo-compressor

The variable geometry turbo-compressor can be divided into three parts: the compressor, the variable geometry turbine and the mechanical coupling.

A.4.1. *Compressor.* The air mass flow rate at the exit of the compressor is expressed by the following semi-empirical equation:

$$\dot{m}_c = \Phi \cdot \frac{p_0}{rT_0} \cdot \frac{\pi}{4} D_c^2 \cdot U_c \quad (\text{A19})$$

$D_c$  is the diameter of the compressor wheel and  $U_c$  is the velocity of the air at the extremity of the compressor's blades. It is proportional to the angular speed of the compressor shaft  $N_{tc}$  and is expressed by

$$U_c = \frac{\pi}{60} \cdot D_c \cdot N_{tc} \quad (\text{A20})$$

$\Phi$  is a correction factor expressed by

$$\Phi = \frac{k_3 \cdot \Psi - k_1}{k_2 + \Psi} \quad (\text{A21})$$

$$k_i = k_{i1} + k_{i2} \cdot M \quad (\text{A22})$$

where  $k_{ij}$  are constants identified from experimental data provided by the variable geometry turbo-compressor constructor.  $M$  is the Mach number; it is the ratio of the blade's velocity  $U_c$  to the velocity of the sound at the entry of the compressor:

$$M = \frac{U_c}{\sqrt{\gamma_a \cdot r \cdot T_0}} \quad (\text{A23})$$

The parameter  $\Psi$  in (A21) is computed using the following equation:

$$\Psi = \frac{C_p T_0 ((\pi_c)^{(\gamma_a - 1)/\gamma_a} - 1)}{0.5 U_c^2} \quad (\text{A24})$$

$\pi_c$  is the compression ratio of the compressor:

$$\pi_c = \frac{p_a}{p_0} \quad (\text{A25})$$

The power consumed by the compressor is expressed by

$$P_c = \dot{m}_c C_p T_0 ((\pi_c)^{(\gamma_a - 1)/\gamma_a} - 1) \frac{1}{\eta_c} \quad (\text{A26})$$

$\eta_c$  is the isentropic efficiency expressed by

$$\eta_c = d_0 + d_1\Phi + d_2\Phi^2 \quad (\text{A27})$$

where  $d_i$  are calculated using the following equation:

$$d_i = d_{i1} + d_{i2} \cdot M + d_{i3} \cdot M^2 \quad (\text{A28})$$

$d_{ji}$  are constants identified from the experimental maps of the compressor.

*A.4.2. Variable geometry turbine.* The gas mass flow rate at the entrance of the turbine,  $\dot{m}_t$  is expressed by the following semi-empirical equation:

$$\frac{\dot{m}_t \cdot \sqrt{T_e}}{p_e \cdot 10^{-3}} = \frac{\sqrt{T_{ech}}}{p_{ech}} \cdot [2 \cdot \pi_t \cdot (1 - \pi_t)]^{0.5} \cdot (h_1 \cdot \text{GV} + h_2) \cdot \left[ h_3 \cdot \left( \frac{1}{\pi_t} - 1 \right) + h_4 \right] \quad (\text{A29})$$

We used this form because the turbochargers maps are usually drawn using the corrected mass flow rate of the turbine  $\{\dot{m}_t \cdot \sqrt{T_e}/(p_e \cdot 10^{-3})\}$ .  $p_{ech}$  and  $T_{ech}$  are the pressure and temperature at the turbine's exit and  $\pi_t$  is the turbine relaxation ratio:

$$\pi_t = \frac{p_0}{p_e} \quad (\text{A30})$$

GV is a real number between 0 and 1, characterizing the change in the inlet guide vane opening which varies the gas effective cross section of the turbine; in the case of a conventional turbo-compressor, it is sufficient to take  $\text{GV} = 0$ . The power produced by the turbine is expressed by

$$P_t = \dot{m}_t C_{pe} T_e (1 - (\pi_t)^{(\gamma_e - 1)/\gamma_e}) \eta_t \quad (\text{A31})$$

$\eta_t$  is the isentropic efficiency of the turbine modeled by

$$\eta_t = k_1 + k_2 \left( \frac{U}{C} \right) + k_3 \left( \frac{U}{C} \right)^2 + k_4 \left( \frac{U}{C} \right)^3 \quad (\text{A32})$$

$k_i$  and  $U/C$  are given by the following equations:

$$k_i = k_{i1} + k_{i2} \cdot N_{tc} + k_{i3} \cdot N_{tc}^2 + k_{i4} \cdot \text{GV} + k_{i5} \cdot \text{GV}^2 + k_{i6} \cdot N_{tc} \cdot \text{GV} \quad (\text{A33})$$

$$\frac{U}{C} = \frac{\pi N_{tc} D_t}{60 \sqrt{2 C_{pe} T_e (1 - (\pi_t)^{(\gamma_e - 1)/\gamma_e})}} \quad (\text{A34})$$

$D_t$  is the diameter of the turbine wheels and  $C_{pe}$  is the heat capacity of air at constant pressure at the temperature  $T_e$ .

*A.4.3. Mechanical coupling.* The fundamental principle of the dynamics applied to the shaft of the turbo-compressor gives

$$I_{tc} w_{tc} \frac{dw_{tc}}{dt} = (\eta_m P_t - P_c) \quad (\text{A35})$$

where  $I_{tc}$  and  $\eta_m$  are, respectively, the moment of inertia and the mechanical efficiency of the turbo-compressor.

## NOMENCLATURE

$w$	engine angular speed (rd/s)
$GV$	opening position of the geometry variable
$P$	pressure (Pa)
$V$	volume ( $m^3$ )
$T$	temperature ( $^{\circ}K$ )
$m'$	mass flow rate (kg/s)
$N_{tc}$	turbo-compressor angular speed (rpm)
$w_{tc}$	turbo-compressor angular speed (rd/s)
$N_{cyl}$	cylinder's number
$V_{cyl}$	displacement ( $m^3$ )
$\eta_v$	inlet air filling efficiency
$\eta_e$	engine effective efficiency
$\eta_{ech}$	heat exchanger efficiency
$\eta_c$	compressor isentropic efficiency
$\eta_t$	turbine isentropic efficiency
$\eta_m$	turbo-compressor mechanical efficiency
$J$	moment of inertia of the engine ( $kg\ m^2$ )
$I_{tc}$	moment of inertia of the turbo-compressor shaft ( $kg\ m^2$ )
$H_f$	lower heating value of fuel (J/kg)
$P_e$	effective power produced by engine (W)
$P_r$	friction power (W)
$C_r$	friction torque (N m)
$\lambda$	air/fuel ratio
$D$	diameter (m)
$M$	mach number
$\pi_c$	compressor/compression ratio
$\pi_t$	turbine relaxation ratio
$r$	mass constant of air (J/(kg OK))
$\gamma$	ratio of heat capacities at constant pressure and volume
$C_p$	heat capacity at constant pressure (J/(kg OK))
B.F.G.S.	Broyden–Fletcher–Goldfarb–Shanno

*Subscripts*

$a$	intake manifold
$e$	exhaust manifold
$c$	compressor
$t$	turbine
$f$	fuel
$0$	atmospheric conditions
max	maximum value

## REFERENCES

1. Amman M, Fekete NP, Guzzella N, Glattfelder AH. Model based control of the VGT and EGR in a turbocharged common rail diesel engine: theory and passenger car implementation. *SAE 2003 World Congress & Exhibition*, Detroit, U.S.A., 2003; 2003-01-0357.
2. Van Nieuwstadt M, Kolmanovsky IV, Moraal PE. Coordinated EGR-VGT control for diesel engines: an experimental comparison. *SAE 2000 World Congress & Exhibition*, Detroit, U.S.A., March 2000; 2000-01-0266.
3. George S, Dixon J. Optimal boost control for an electrical supercharging application. *SAE 2004 World Congress*, Detroit, U.S.A., March 2004; 2004-01-0523.
4. Olsson L, Abul-Milh M, Karlsson H, Jobson E, Thormahlen P, Hinz A. The effect of a changing lean gas composition on the ability of NO<sub>2</sub> formation and NO<sub>x</sub> reduction over supported Pt catalysts. *Topics in Catalysis* 2004; **30–31**(1):85–90. DOI: 10.1023/B:TOCA.0000029733.75156.25.
5. Mital R, Li J, Huang SC, Stroia BJ, YU RC, Howden KC. Diesel exhaust emissions control for light duty vehicles. *SAE 2003 World Congress & Exhibition*, Detroit, U.S.A., March 2003; 2003-01-0041.
6. Bai L, Yang M. Coordinated control of EGR and VNT in turbocharged diesel engine based on intake air mass observer. *SAE 2002 World Congress & Exhibition*, Detroit, U.S.A., March 2002; 2002-01-1292.
7. Stefanopoulou A, Kolmanovsky IV, Freudenberg JS. Control of variable geometry turbocharged diesel engines for reduced emissions. *Control Systems Technology* 2000; **8**(4):733–745. DOI: 10.1109/87.852917.
8. Moorai P, Kolmanovsky I. Turbocharger modeling for automotive control applications. *SAE 1999 World Congress & Exhibition*, Detroit, U.S.A., 1999; 1999-01-0908.
9. Younes R, Champoussin JC. *Le Turbocompresseur à Géométrie Variable, un Moyen de Réduire la Pollution*. Journées SFT: Paris, France, 1994.
10. Younes R. Elaboration d'un modèle de connaissance du moteur diesel avec turbocompresseur à géométrie variable en vue de l'optimisation de ses émissions. *Ph.D. Thesis*, Ecole Centrale de Lyon, France, 1993.
11. Jung M. Mean value modelling and robust control of the airpath of a turbocharged diesel engine. *Ph.D. Thesis*, University of Cambridge: U.K., 2003.
12. Dovifaaz X. Modélisation et commande de moteur diesel en vue de la réduction de ses émissions. *Ph.D. Thesis*, Université de Picardis Jules Vernes, France, 2000.
13. Minoux M. *Programmation Mathématique: Théorie et Algorithmes*. Dunod, France, 1983; ISBN: 2040154876.
14. Michel S, Maignan D, Collette Y, Martini E, Bachler J, Weber M. Dynamic tuning: a new approach for fast engine emission calibration. *SIA International Conference*, Lyon, France, May 2006.
15. Brahma I, Rutland CJ. Improvement of neural network accuracy for engine simulations. *SAE Powertrain & Fluid Systems Conference & Exhibition*, Pittsburgh, U.S.A., October 2003; 2003-01-3227.
16. Filipi ZF, Wu B, Assanis DN, Kramer DM, Ohl GL, Prucka MJ, DiValentin E. Using artificial neural networks for representing the air flow rate through a 2.4 liter VVT engine. *SAE Powertrain & Fluid Systems Conference & Exhibition*, Tampa, U.S.A., October 2004; 2004-01-3054.
17. Traver ML, Atkinson CM, Atkinson RJ. Neural network-based diesel engine emissions prediction using in-cylinder combustion pressure. *International Fuels & Lubricants Meeting & Exposition*, Dearborn, U.S.A., May 1999; 1999-01-1532.
18. Zweiri YH. Diesel engine indicated torque estimation based on artificial neural networks. *International Journal of Intelligent Technology* 2006; **1**(3):233–239.
19. Hafner M. Model based determination of dynamic engine control function parameters. *International Spring Fuels & Lubricants Meeting*, Orlando, U.S.A., May 2001; 2001-01-1981.